Eur. Phys. J. B (2022)95:31
https://doi.org/10.1140/epjb/s10051-022-00295-z

THE EUROPEAN PHYSICAL JOURNAL B

Regular Article - Mesoscopic and Nanoscale Systems

Dielectric function and impurity-limited mobility of semiconductor quantum wires: effects of dielectric mismatch and finite confining potential

Nguyen Nhu Dat[1,2,3,a] and Nguyen Thi Thuc Hien[1,b]

[1] Institute of Theoretical and Applied Research, Duy Tan University, 1 Phung Chi Kien, Hanoi 100000, Vietnam
[2] Faculty of Natural Sciences, Duy Tan University, 3 Quang Trung, Da Nang 550000, Vietnam
[3] Institute of Physics, Vietnam Academy of Science and Technology, 10 Dao Tan, Hanoi 100000, Vietnam

Received 4 December 2021 / Accepted 6 February 2022

Abstract. The dielectric response function of the electron system in a cylindrical semiconductor quantum wire (QWR) embedded in a dielectric material is derived within the random phase approximation in the quantum limit when only the lowest electron subband is considered. The wire is studied in both finite and infinite confining potential models. It is shown that the dielectric mismatch strongly affects the collective excitations of the electron system and the electrostatic interaction between charged particles in the wire. The electron screening is greatly enhanced in thin QWRs with low-κ dielectric surroundings and weakened for high-κ dielectric environment. Thus, the impurity-limited electron mobility can be improved in small-radius semiconductor QWRs coated with a material having a dielectric constant smaller than that of the semiconductor, as opposed to a number of previous reports. The calculations also indicate that the model of infinite potential barrier for thin QWRs underestimates the impurity electron mobility compared to the finite barrier model and can be used in the case of QWRs with large radii.

1 Introduction

The quasi-one-dimensional semiconductor structures, i.e., *quantum wires* (QWRs), have attracted increasing attention from both experimental and theoretical points of view because of their possible applications in opto-electronic and microelectronic devices such as quantum wire lasers [1–5], light-emitting diodes [6–9], quantum waveguide inverters [10,11], quatum wire transistors [12–16], memory elements [17,18], and chemical and biological sensors [19–21]. Factors that affect the performance of these devices include the dielectric properties of semiconductor structures [22].

Semiconductor quantum wires are usually surrounded with materials having the dielectric constant different from that of the wire material. A number of studies on the dielectric mismatch effect have been reported. It was demonstrated that an outer dielectric environment changes the Coulomb interaction in QWRs, leading to considerable variations in hydrogenic impurity binding energies [23–25]. The distorted Coulomb interaction between charge carriers results in a very large increase in the exciton binding energy which is of order of room temperature thermal energy [26–32]. The existence of a two-electron bound state in a silicon deformed quantum wire was pointed out in [33], depending on the wire shape. It has also been shown that the dielectric mismatch still supports two-electron localized states for considered wire geometries, although the absolute value of the ground-state binding energy is less than that without dielectric effects. Konar et al. [34–36] have analyzed the effect of the dielectric constant mismatch on the free-carrier screening and impurity scattering of electrons in QWRs. The authors have showed that an environment with a dielectric constant higher than that of the wire can reduce the free-carrier screening and, conversely, a lower κ surroundings can enhance the dielectric function of the system [36]. The authors also indicated an improvement of the impurity-limited mobility of electrons by at least one order of magnitude in QWRs embedded in a medium with higher dielectric constant [34,35]. The point is that the stronger the screening the weaker the electrostatic interaction between charged particles and it is expected that the impurity mobility can be improved in QWRs with a lower κ surroundings, contrary to the conclusion reported in [34,35]. Therefore, it is worth reconsidering the effect of dielectric mismatch on the electron screening and impurity mobility in QWRs. In addition, the assumption of an infinite potential barrier was adopted in the mentioned works. Machado et al. considered the effects of the confining potential height

[a] e-mails: nguyennhudat@duytan.edu.vn; nndat@iop.vast.vn (corresponding author)
[b] e-mail: hien49@gmail.com

for a GaAs/$Al_xGa_{1-x}As$ quantum wire, neglecting the dielectric properties of the system, and pointed out that the height of the potential has a remarkable influence on the plasmon energy of a quasi-one-dimensional electron gas (Q1DEG) in the QWR [37]. In the case of the finite potential barrier height, the electron wave function spreads into the barrier region and the free-carrier screening can be modified. Therefore, in the present paper, we investigate the effects of both the dielectric constant mismatch and the finite height of the confining potential on electronic properties of such QWRs.

In Sect. 2, applying the random-phase approximation (RPA), we derive the dielectric function for the Q1DEG in the cylindrical quantum wire (CQWR) surrounded by the medium with a different dielectric constant. The intrasubband plasmon dispersion is obtained as a root of the dielectric function. The charged impurity-limited mobility of electrons is presented in Sect. 3. Our results are summarized in Sect. 4.

2 Free-carrier screening and collective excitations of a Q1DEG

We consider a free-electron gas in a cylindrical semiconductor quantum wire of length L (assumed large) and radius R made of a material with dielectric constant ε_1. The wire is embedded in a homogeneous infinite medium (barrier region) with dielectric constant ε_2. The electrons are assumed to move freely along the wire axis (chosen as the z-axis) and confined in the lateral direction by a potential given as

$$V(r) = \begin{cases} 0 & \text{for } r \le R \\ V_0 > 0 & \text{for } r > R. \end{cases} \tag{1}$$

Here, $r = |\mathbf{r}|$ with $\mathbf{r}$ being a position in (x, y)-plane. For simplicity, the electron effective mass m^* is assumed to be the same in the wire and in the surroundings. The motion of an electron in the wire is affected not only by the confining potential (1) but also in general by its image potential arising from the difference in dielectric constants of the wire and the surrounding materials. From symmetry of the wire, it follows that the image potential depends only on the distance $r = |\mathbf{r}|$ from the wire axis for an electron at point $\mathbf{x} = (\mathbf{r}, z)$. This was actually verified by calculation [33]. That means the dielectric mismatch does not affect the free motion of the electron along the z-axis.

Within the effective mass approximation, the electron envelope wave function for bounded states can be written in cylindrical coordinates (r, θ, z) as

$$\Psi_{l,n,k}(\mathbf{x}) \equiv \langle \mathbf{x}|l, n, k\rangle = \frac{1}{\sqrt{2\pi L}}\, \mathrm{e}^{i(l\theta + kz)}\, \phi_{l,n}(r). \tag{2}$$

The image potential can affect the electron motion in the plane perpendicular to the wire axis. As pointed out in [38], the change of the electron radial wave function $\phi_{l,n}(r)$ by the image potential is negligible, especially for quantum wires with small radii. Therefore, for simplicity, we ignored the image charge effects on the lateral motion of electron.

In the case of finite V_0, the radial part $\phi_{l,n}(r)$ of the wave function has the form

$$\phi_{l,n}(r) = \begin{cases} A\, J_l(\upsilon r) & \text{for } r \le R \\ B\, K_l(\kappa r) & \text{for } r > R \end{cases} \tag{3}$$

and the energy eigenvalue $E_{l,n}(k)$ is

$$E_{l,n}(k) = E_{l,n} + \frac{\hbar^2 k^2}{2m^*}, \tag{4}$$

Here, A and B are constants defined by the normalization and continuity of the eigenfunctions. $J_l(x)$ is the Bessel function of the first kind of order l and $K_l(x)$ is the modified Bessel function of the second kind [39].

The quantities υ and κ are related to the energy $E_{l,n}$ and given by

$$\upsilon = \sqrt{\frac{2m^*}{\hbar^2} E_{l,n}}, \quad \kappa = \sqrt{\frac{2m^*}{\hbar^2} (V_0 - E_{l,n})}. \tag{5}$$

The energy $E_{l,n}$ is specified by quantum numbers (l, n) as subband indexes and defined by a root of the equation

$$\upsilon J_l'(\upsilon R) K_l(\kappa R) - \kappa J_l(\upsilon R) K_l'(\kappa R) = 0, \tag{6}$$

where n denotes the n-th root of the equation, and $J_l'(x)$ $(K_l'(x))$ is the derivative of function $J_l(x)$ $(K_l(x))$ with respect to argument x.

For infinite V_0, the radial part of the wave function and the energy for electrons are

$$\phi_{l,n}(r) = \begin{cases} \frac{\sqrt{2}}{R J_{l+1}(x_{l,n})} J_l\left(x_{l,n} \frac{r}{R}\right) & \text{for } r \le R \\ 0 & \text{for } r > R \end{cases} \tag{7}$$

and

$$E_{l,n}(k) = E_{l,n} + \frac{\hbar^2 k^2}{2m^*} \quad \text{with} \quad E_{l,n} = \frac{\hbar^2}{2m^*} \left(\frac{x_{l,n}}{R}\right)^2, \tag{8}$$

respectively. Here, $x_{l,n}$ is the n-th zero of the Bessel function $J_l(x)$ of order l.

To investigate the response of a Q1DEG in a CQWR to an external longitudinal electric field and plasmon excitations in the system, we follow the formalism proposed by Ehrenreich and Cohen [40] known as the self-consistent field approach or RPA. This approach provides a good description for intrasubband plasmon dispersion in QWRs as shown in Ref. [41]. When applied an external perturbation $V_0(\mathbf{x}, t) = V_0(\mathbf{x}) \exp(-i\omega t)$ to the Q1DEG, a change $\delta n(\mathbf{x}, t)$ in the electron density from its equilibrium value is induced, creating a screening potential $V_s(\mathbf{x}, t)$. The self-consistent potential $V(\mathbf{x}, t)$ is composed of the external potential $V_0(\mathbf{x}, t)$ and the screening potential $V_s(\mathbf{x}, t)$. The time

dependence of all the potentials is assumed the same and the steady-state quantities of the system will be calculated at $t = 0$.

Neglecting retardation effects, the screening potential $V_s(\mathbf{x})$ is defined by Poisson's equation

$$\nabla^2_{\mathbf{x}}\, V_s(\mathbf{x}) = -\frac{4\pi e^2}{\varepsilon(r)}\delta n(\mathbf{x}) \tag{9}$$

where

$$\varepsilon(r) = \begin{cases} \varepsilon_1 & \text{for } r \le R \\ \varepsilon_2 & \text{for } r > R, \end{cases}$$

$(-e)$ is the electron charge. Within the linear response theory and the RPA the induced charge density is given by

$$\delta n(\mathbf{x}) = \sum_{\alpha\alpha'} \langle\alpha|\delta\rho|\alpha'\rangle\, \Psi^*_{\alpha'}(\mathbf{x})\Psi_{\alpha}(\mathbf{x}), \tag{10}$$

where α (α') denotes the set of quantum numbers l, n, k (l', n', k'). $\delta\rho$ is the correction to the single particle density operator to first order in the potential V and its matrix element is given by

$$\langle\alpha|\delta\rho|\alpha'\rangle = \frac{f_0(E_\alpha) - f_0(E_{\alpha'})}{E_\alpha - E_{\alpha'} - \hbar\omega - i\gamma}\, \langle\alpha|V|\alpha'\rangle \tag{11}$$

with $f_0(E_\alpha)$ being the Fermi–Dirac distribution function. γ is the phenomenological parameter introduced to take into account the broadening of electron energy levels due to different scattering processes.

We introduce the one-dimensional Fourier transform of the screening potential $V_s(\mathbf{x})$ and the self-consistent potential $V(\mathbf{x})$:

$$\widetilde{V}_s(\mathbf{r}, q) = \frac{1}{L}\int \mathrm{d}z\ \mathrm{e}^{-iqz}\, V_s(\mathbf{r}, z), \tag{12}$$

$$\widetilde{V}(\mathbf{r}, q) = \frac{1}{L}\int \mathrm{d}z\ \mathrm{e}^{-iqz}\, V(\mathbf{r}, z). \tag{13}$$

Substituting (10), (11) and (12) into (9), we obtain the equation for the Fourier component $\widetilde{V}_s(\mathbf{r}, q)$ of the screening potential

$$\begin{aligned}\left(\nabla^2_{\mathbf{r}} - q^2\right)\widetilde{V}_s(\mathbf{r}, q) &= -\frac{2e^2}{L\varepsilon(r)}\sum_{l,n,l',n'} \langle l, n, q|V|l', n', 0\rangle \\ &\quad\times\Pi^{l,n}_{l',n'}(q,\omega)\ \mathrm{e}^{i(l-l')\theta}\ \phi^*_{l',n'}(r)\phi_{l,n}(r),\end{aligned} \tag{14}$$

where

$$\Pi^{l,n}_{l',n'}(q,\omega) = \sum_k \frac{f_0(E_{l,n}(k+q)) - f_0(E_{l',n'}(k))}{E_{l,n}(k+q) - E_{l',n'}(k) - \hbar\omega - i\gamma}$$

is the Lindhard function (polarization function). The Green's function for the above equation, satisfying the equation

$$\left(\nabla^2_{\mathbf{r}} - q^2\right) G(q; \mathbf{r}, \mathbf{r}') = -\delta(\mathbf{r} - \mathbf{r}')\ , \tag{15}$$

is [42]

$$G(q; \mathbf{r}, \mathbf{r}') = \frac{1}{2\pi}\sum_{m=-\infty}^{\infty} \mathrm{e}^{im(\theta-\theta')}\, g_m(q; r, r') \tag{16}$$

with

$$g_m(q; r, r') = I_m(qr_<)K_m(qr_>). \tag{17}$$

Here, we use the notation $r_{<(>)} = \min(\max)\{r, r'\}$, $I_m(x)$ is the modified Bessel function of the first kind of order m. Using the above Green's function, the screening potential can be written as

$$\begin{aligned}\widetilde{V}_s(\mathbf{r}, q) = \frac{2e^2}{L}&\sum_{l,n,n',m} \langle l+m, n', q|V|l, n, 0\rangle\ \mathrm{e}^{im\theta} \\ &\times\Pi^{l+m,n'}_{l,n}(q,\omega)\int \mathrm{d}r' r' \left\{\frac{1}{\varepsilon(r')}g_m(q; r, r') \right. \\ &\left. + \left(\frac{1}{\varepsilon_2} - \frac{1}{\varepsilon_1}\right) U_m(q; r, r')\right\} \phi^*_{l,n}(r')\phi_{l+m,n'}(r')\end{aligned} \tag{18}$$

where

$$\begin{aligned}U_m(q; r, r') \ = &\left[(\varepsilon_2/\varepsilon_1)K'_m(qR)I_m(qr')\Theta(R - r')\right. \\ &\left.+I'_m(qR)K_m(qr')\Theta(r' - R)\right] \\ &\times\left[K_m(qR)I_m(qr)\Theta(R - r)\right. \\ &\left.+I_m(qR)K_m(qr)\Theta(r - R)\right] \\ &\times\left[(\varepsilon_2/\varepsilon_1)K'_m(qR)I_m(qR)\right. \\ &\left.-I'_m(qR)K_m(qR)\right]^{-1},\end{aligned}$$

where $\Theta(x)$ being the Heaviside step function.

Since we are interested in intrasubband collective excitations, we consider only the lowest subband $(0, 1)$. This is applicable for QWRs in the size quantum limit. The dielectric response function is defined as $\epsilon = \langle V_0\rangle/\langle V\rangle$. From (18), we obtain the dielectric function for the Q1DEG in the quantum wire

$$\begin{aligned}\epsilon(q,\omega) &= 1 - \frac{\langle 0, 1, q|V_s|0, 1, 0\rangle}{\langle 0, 1, q|V|0, 1, 0\rangle} \\ &= 1 - \frac{2e^2}{L}\Pi^{0,1}_{0,1}(q,\omega)\, F(q),\end{aligned} \tag{19}$$

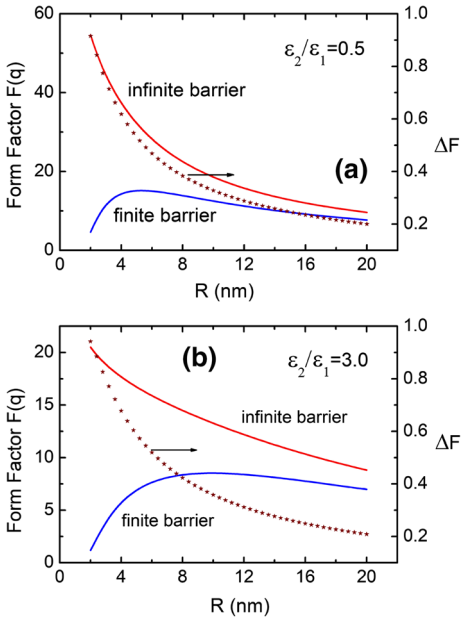

Fig. 1 The form factor for a quantum wire with finite or infinite confining potential as a function of wire radius for the ratio of dielectric constants **a** $\varepsilon_2/\varepsilon_1 = 0.5$, **b** $\varepsilon_2/\varepsilon_1 = 3.0$ (solid line). Asterisks show the radius dependence of the relative difference of form factors. The linear electron density is $n = 10^6\,\mathrm{cm}^{-1}$, the wave vector $q = 10^6\,\mathrm{cm}^{-1}$, the temperature of the system $T = 300\,\mathrm{K}$

where the form factor $F(q)$ is given by

$$F(q) = \int \mathrm{d}r \int \mathrm{d}r'\; rr'\,\phi^*_{0,1}(r)\phi_{0,1}(r)\phi^*_{0,1}(r')\phi_{0,1}(r') \times \left\{ \frac{1}{\varepsilon(r')} g_0(q;r,r') + \left(\frac{1}{\varepsilon_2} - \frac{1}{\varepsilon_1}\right) U_0(q;r,r') \right\}. \tag{20}$$

The form factor $F(q)$ takes into account the effects of both the confining potential and the dielectric mismatch.

All the numerical calculations in this work are performed for a GaAs quantum wire with the following values: $\varepsilon_1 = 12.9$, $m^* = 0.063\,m_e$ with m_e being the free electron mass. The parameter γ is chosen to be $10^{-4}E_F$ where E_F is the Fermi energy [43], the barrier height $V_0 = 237\,\mathrm{mV}$.

In Fig. 1, we present the change of the form factor $F(q)$ as the wire radius R changes for different values of the ratio $\varepsilon_2/\varepsilon_1$ for two models of the confining potential: finite and infinite barriers. It can be seen that $F(q)$ gradually decreases with increasing wire radius for infinite barriers, while for finite barriers it reaches a maximum at some radius value and then decreases. Figure 1 also illustrates the radius dependence of the relative difference of form factors ΔF, i.e., the difference of the form factors for finite and infinite potential barriers compared to the form factor for the infinite barrier. It is seen that ΔF varies with radius R in almost the same way for different values of ratio $\varepsilon_2/\varepsilon_1$ and the larger the radius, the smaller the relative difference. The relative difference is approximately 0.6, 0.3, and 0.2 for radius of 4, 12, and 20 nm, respectively. This means that the model of infinite barrier height is applicable to large radius quantum wires regardless of the ratio $\varepsilon_2/\varepsilon_1$.

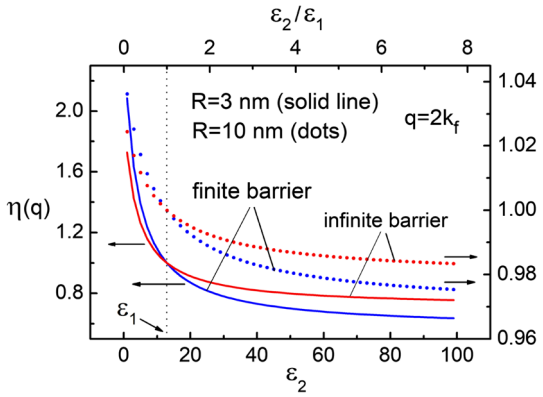

Fig. 2 Dependence of the measure of the effect of dielectric mismatch on dielectric constant ε_2 for a quantum wire calculated in both two models of confining potentials. The linear electron density is $n = 10^6\,\mathrm{cm}^{-1}$, the temperature of the system $T = 300\,\mathrm{K}$

We define the quantity $\eta(q)$ which is the ratio of the form factor $F(q)$ for a wave vector q calculated for a quantum wire embedded in a medium with a dielectric constant ε_2 and the form factor $F(q)$ for the same quantum wire coated with a medium having $\varepsilon_2 = \varepsilon_1$. The ratio represents the measure of the effect of dielectric mismatch on the form factor. The more this ratio differs from 1, the stronger the effect of dielectric mismatch. The dependence of η on dielectric constant ε_2 for QWRs of radii of 3 and 10 nm is plotted in Fig. 2.

The figure indicates that the effect of dielectric mismatch is stronger for quantum wires with low-κ dielectric surrounding media ($\varepsilon_2 < \varepsilon_1$). The quantity η differs more from 1 in the model of finite potential barrier than in the model of infinite barrier. In addition, the measure η is approximately 25% different from 1 for the QWR with a radius of 3 nm and 3% for $R = 10\,\mathrm{nm}$. This means the dielectric mismatch is more effective in QWRs with a small radius and in the finite barrier model.

Since the polarization function $\Pi^{0,1}_{0,1}(q,\omega)$ is independent of the dielectric properties of the system, the dielectric mismatch affects the dielectric function (19) through the form factor (20). In Fig. 3 the curves describe the static dielectric function of a QWR as a function of the dielectric constant ε_2 of the surroundings for QWRs with different radii.

The static screening decreases strongly with increasing ε_2 in the range of $\varepsilon_2 < \varepsilon_1$. For larger ε_2, the screening is slowly decreasing and approaches a constant. The change in the screening in the considered range of ε_2 is noticeable for thin QWRs and is small for QWRs of large lateral size. This fact indicates again that the effect of the dielectric mismatch is more pronounced for

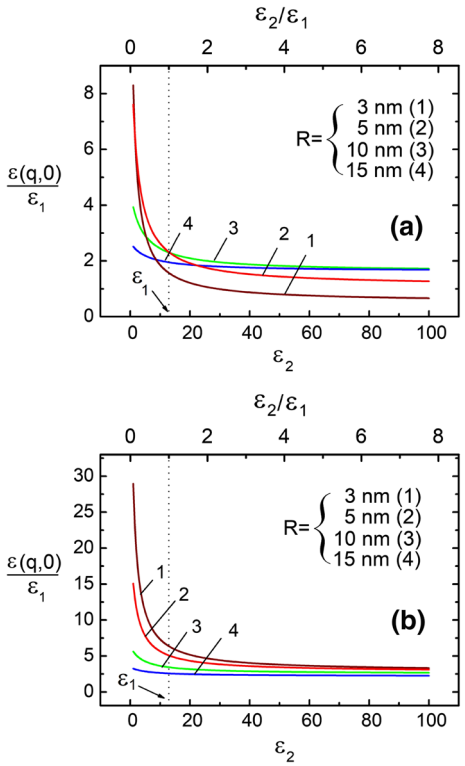

Fig. 3 Static dielectric function as a function of dielectric constant ε_2 of the surrounding environment for quantum wires of different radii with **a** finite potential barrier or **b** infinite barrier. The linear electron density is $n = 10^6\,\mathrm{cm}^{-1}$, the wave vector $q = 10^6\,\mathrm{cm}^{-1}$, the temperature of the system $T = 300\,\mathrm{K}$

QWRs with small radius and low-κ dielectric surroundings.

Regarding the dependence on QWR radius, we plotted in Fig. 4 the static dielectric function as a function of QWR radius for several values of the ratio $\varepsilon_2/\varepsilon_1$. The screening is a decreasing function of the QWR radius for all values of ratio $\varepsilon_2/\varepsilon_1$ in the model of infinite potential barrier, while this does not apply to the finite barrier height model. In the later model, the dielectric function has a maximum at a small radius. The smaller the $\varepsilon_2/\varepsilon_1$ ratio, the more pronounced the maximum. As the ratio $\varepsilon_2/\varepsilon_1$ increases, the peak blurs and its position shifts to larger radii. For both models of confining potential, the dielectric function decreases with increasing wire radius in the range of large radii, tending to a limit which is almost the same for all values of $\varepsilon_2/\varepsilon_1$. This means the effect of dielectric mismatch weakens with increasing radius of the QWR and is washed away in QWRs of a large radius.

The dispersion of collective longitudinal electronic excitations (called plasmons) in a Q1DEG is obtained as a root of the dynamical dielectric function, $\epsilon(q,\omega) = 0$.

The curves in Fig. 5a represent the plasmon dispersion calculated for both models of confining potentials for a quantum wire embedded in a medium with

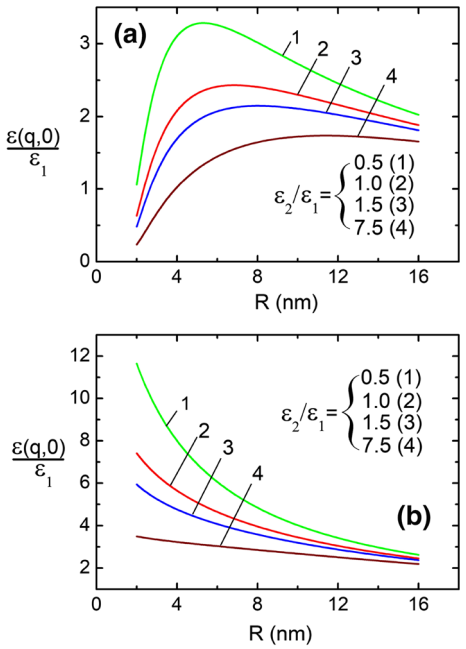

Fig. 4 Static dielectric function as a function of QWR radius for a quantum wire with **a** finite potential barrier or **b** infinite barrier for different values of the ratio $\varepsilon_2/\varepsilon_1$. The linear electron density is $n = 10^6\,\mathrm{cm}^{-1}$, the wave vector $q = 10^6\,\mathrm{cm}^{-1}$, the temperature of the system $T = 300\,\mathrm{K}$

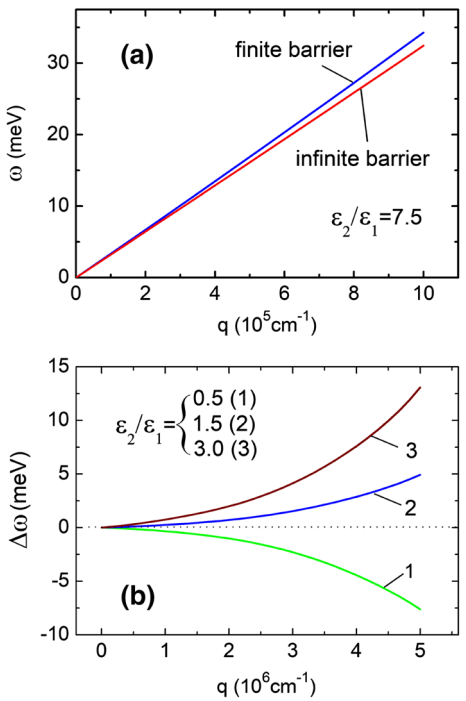

Fig. 5 **a** Plasmon dispersion in a QWR in the models of finite and infinite confining potentials and **b** deviation of plasma frequencies of a QWR in a surrounding environment of dielectric constant $\varepsilon_2 \neq \varepsilon_1$ from the plasma frequencies in the case with $\varepsilon_2 = \varepsilon_1$ in the model of finite potential barrier. The radius of the QWR is $R = 3\,\mathrm{nm}$, the linear electron density is $n = 10^6\,\mathrm{cm}^{-1}$, the temperature of the system $T = 300\,\mathrm{K}$

$\varepsilon_2/\varepsilon_1 = 7.5$. In the long-wavelength limit, the plasma frequency is linearly dependent on the wave vector q and is reduced to zero, as experimentally found in [44]. The plasma frequency in the model of finite potential barrier is higher than in the infinite barrier model. The frequency difference is 2 meV at $q = 10^6\,\mathrm{cm}^{-1}$ and higher at larger wave vectors. For collective excitations in the Q1DEG, the electrostatic interaction between electrons and background positive charges plays a role of the restoring force. The stronger the restoring force, the higher frequency of the collective oscillation. As seen from Ref. [30], the Coulomb potential of a charge located in the wire changes little in the wire region with a change in ε_2 (i.e., is almost independent of ε_2). On the other hand, the wave function for electrons in the lowest subband is confined mostly in the wire (moreover, in the vicinity of the wire axis in the case of an infinite confining potential) [29]. Therefore, the interaction between electrons and the positive background in the wire changes mainly by the free-electron screening as ε_2 changes. Since the free-electron screening increases with decreasing dielectric constant ε_2 of surroundings as seen in Fig. 3a, resulting in weakening the interaction between charged particles, it is expected that the plasma frequency is lower in QWRs surrounded by lower κ media. It actually happened as Fig. 5b showed, where the difference of the plasma frequency in the QWR coated with a ε_2-dielectric environment from the plasma frequency of the dielectric homogeneous QWR (i.e., with $\varepsilon_2 = \varepsilon_1$) is plotted as a function of wave vector q. The calculation was performed for the model of finite potential barrier. The result is similar for the infinite potential barrier model. This mode softening with decreasing dielectric constant ε_2 is in contrast to what is given in [36] according to which the mode has softened with increasing dielectric constant of the surrounding media (see Fig. 2b therein).

In Fig. 6, we plotted the dependence of plasma frequency $\omega(q)$ on the QWR radius in both models of confining potentials. From the figure, it is clear to see the influence of the height of the potential barrier on the variation of the plasma frequency with the QWR size.

In the case of an infinite barrier height, the plasma frequency increases gradually with the radius of the QWR. Meanwhile, the radius dependence of plasma frequency for QWRs with a finite potential barrier is quite different. The plasma frequencies decrease rapidly with the QWR size within small radii and then increase slowly. This is due to the different size dependence of the electron screening in the two models of confining potentials illustrated in Fig. 4, which results in different dependence on QWR radius of restoring force for plasmons. For both models of confining potential, plasma frequencies tend to the same limit in QWRs of large lateral size despite the dielectric constant ε_2 of the surrounding environment. This means that the dielectric mismatch is ineffective in QWRs of large radii.

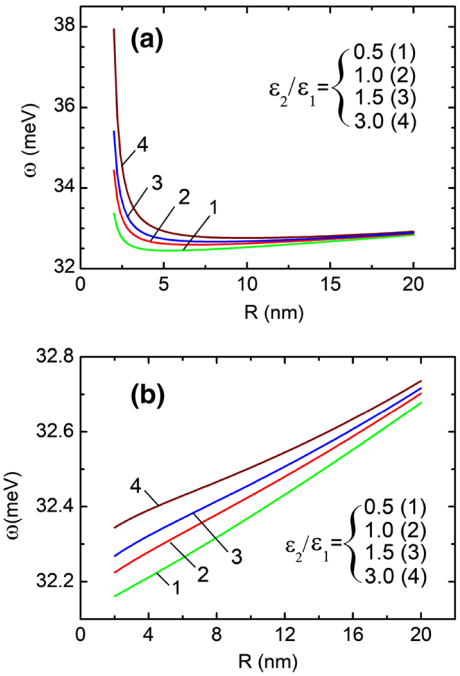

Fig. 6 Plasma frequency for a fixed $q = 10^6\,\mathrm{cm}^{-1}$ as a function of the QWR radius for different values of the ratio $\varepsilon_2/\varepsilon_1$ in the model of confining potential with barrier height **a** finite and **b** infinite. The linear electron density is $n = 10^6\,\mathrm{cm}^{-1}$, the temperature of the system $T = 300\,\mathrm{K}$

3 Impurity-limited mobility of a CQWR

We assume that the electrons in a CQWR are scattered by an impurity of charge e located on the axis of the wire. Without loss of generality, the impurity position can be taken as the origin of the coordinate system. The electrostatic potential $\varphi(\mathbf{x})$ of the ionized impurity is a solution of Poisson's equation

$$\nabla^2_{\mathbf{x}}\ \varphi(\mathbf{x}) = \frac{4\pi e}{\varepsilon(r)}\delta(\mathbf{x}). \tag{21}$$

The Fourier component of the function $\varphi(\mathbf{x})$ respect to z is given by

$$\begin{aligned}\widetilde{\varphi}(\mathbf{r}, q) &= -\frac{4\pi e}{\varepsilon_1 L}\Bigg\{K_0(qr) + \frac{(\varepsilon_1 - \varepsilon_2)\ K_0'(qR)}{\varepsilon_2 K_0'(qR)\, I_0(qR) - \varepsilon_1 K_0(qR)\, I_0'(qR)} \\ &\quad \times \left[\Theta(R-r)K_0(qR)I_0(qr) + \Theta(r-R)I_0(qR)K_0(qr)\right]\Bigg\}.\end{aligned} \tag{22}$$

It is seen that the dielectric inhomogeneity is captured in the second term in braces.

The electron mobility μ is given as

$$\mu\ =\ \frac{e}{m^*}\,\tau. \tag{23}$$

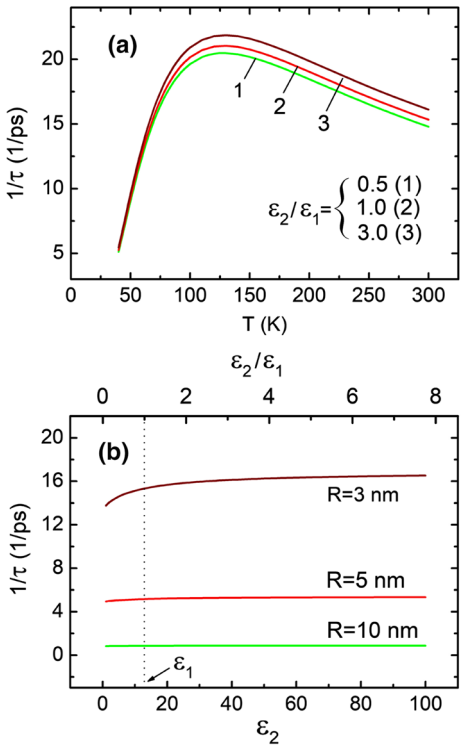

Fig. 7 Ionized-impurity scattering rate **a** as a function of temperature for a QWR of 3 nm radius for several values of ratio $\varepsilon_2/\varepsilon_1$ and **b** as a function of dielectric constant ε_2 for various radii of QWRs at temperature $T = 300\,\mathrm{K}$. The calculation was performed for QWRs in the model of finite potential barrier. The linear electron density is $n = 10^6\,\mathrm{cm}^{-1}$, the linear impurity density $c_i = 10^6\,\mathrm{cm}^{-1}$

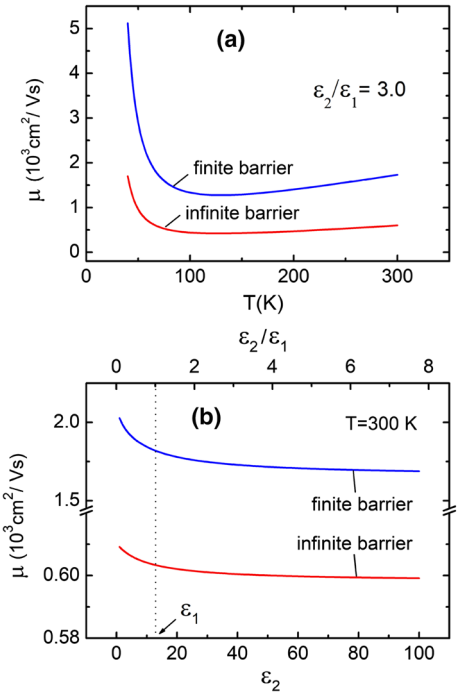

Fig. 8 Impurity-limited electron mobility **a** as a function of temperature for ratio $\varepsilon_2/\varepsilon_1 = 3.0$ and **b** as a function of dielectric constant ε_2 at temperature $T = 300\,\mathrm{K}$. The calculation was performed for QWRs in both models of confining potentials. The linear electron density is $n = 10^6\,\mathrm{cm}^{-1}$, the linear impurity density $c_i = 10^6\,\mathrm{cm}^{-1}$, the wire radius $R = 3\,\mathrm{nm}$

where τ denotes the relaxation time describing electron momentum decay due to scattering of various kinds. The Hamiltonian for scattering of electrons by ionized impurities is

$$H_{int} = -\frac{e}{\epsilon}\,\varphi(\mathbf{x}), \tag{24}$$

where ϵ is the dielectric function (19) reflecting the screening by free electrons in the QWR and the dielectric mismatch. To calculate the relaxation time τ, we adopt the memory function formalism proposed by Götze and Wölfle [45]. In the size quantum limit, we obtain the expression for the electron relaxation time limited by impurity scattering

$$\frac{1}{\tau} = \frac{16\pi\hbar c_i}{m^* n k_B T}\sum_{kk'}(k-k')^2\left|\langle 0,1,k|H_{int}|0,1,k'\rangle\right|^2 \times f_0(E_{0,1}(k'))\left[1-f_0(E_{0,1}(k))\right]\delta(E_{0,1}(k')-E_{0,1}(k)). \tag{25}$$

Here, c_i is the linear density of impurities, k_B the Boltzmann constant.

The temperature dependence of the charged-impurity scattering rate calculated for a thin QWR with a finite potential barrier is depicted in Fig. 7a. At low temperatures, the scattering rate is almost independent of the dielectric constant ε_2 of the surroundings of the QWR and increases with temperature. The scattering rate is then a decreasing function at high temperatures and its value is affected by the dielectric constant ε_2. However, the dielectric mismatch is effective only in QWRs of small radii, as seen in Fig. 7b, where the scattering rate as a function of ε_2 is shown for QWRs of different radii. The scattering rate increases with the dielectric constant ε_2 and its variation for ε_2 in the range from 1 to 100 is 20% and 6% for $R = 3$ and 10 nm, respectively, where a large change occurs for $\varepsilon_2 < \varepsilon_1$. The ε_2 dependence of the scattering rate is consistent with the dependence of the electron screening on the dielectric constant ε_2 illustrated in Fig. 3a. From the same arguments as for the ε_2 dependence of the plasma frequencies, the reduction of the screening with increasing ε_2 results in the increase of the screened electric potential of charged impurities seen by electrons, leading to an increase in the impurity scattering rate with the dielectric constant ε_2. It should be noted that this ε_2 dependence of the scattering rate is in contrast to that reported in [35,36] (see figures numbered 3 therein) according to which the scattering rate decreases with increasing ε_2.

We plotted the impurity-limited electron mobility as a function of temperature in Fig. 8a and as a func-

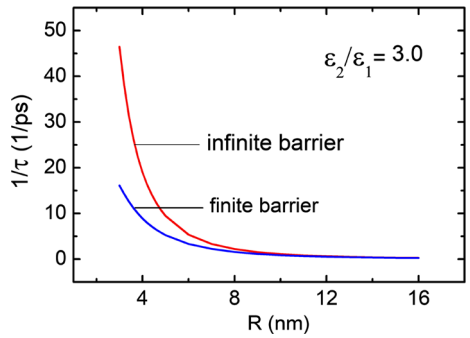

Fig. 9 Coulomb scattering rate as a function of QWR radius calculated in both models of confining potential. The linear electron density is $n = 10^6\,\mathrm{cm}^{-1}$, the linear impurity density $c_i = 10^6\,\mathrm{cm}^{-1}$, the ratio of dielectric constants $\varepsilon_2/\varepsilon_1 = 3.0$, the temperature $T = 300\,\mathrm{K}$

tion of dielectric constant ε_2 in Fig. 8b for a QWR of 3 nm radius. The calculation is for a QWR with a finite or infinite potential barrier. The mobility decreases rapidly at low temperatures and in the range of $\varepsilon_2 < \varepsilon_1$. This behavior is the same for both models of confining potentials, but the impurity mobility is approximately four times greater in the finite barrier model in comparison with the infinite barrier model. In Fig. 9, the Coulomb scattering rate is plotted as a function of QWR radius for both finite and infinite barrier height models. The scattering rate in the later model is higher than in the first model for QWRs with a radius of less than 10 nm and is the same for larger QWRs. The results show the infinite barrier model underestimates (overestimates) the impurity-limited mobility (the Coulomb scattering rate) in QWRs of small radii and is applicable for QWRs with large radii.

4 Conclusion

In summarizing, we have calculated the dielectric function for a quasi-one-dimensional electron gas in a cylindrical semiconductor quantum wire coated with a dielectric material, taking into account the difference in dielectric constants of the wire and the surroundings. It is assumed that electrons are confined in the lateral direction by a potential well of finite or infinite height and have the same effective mass in the core and the surrounding material. It was found that the effect of the dielectric mismatch on electron screening, plasmon dispersion and charged-impurity scattering rate of electrons is significant in thin QWRs with low-κ surrounding materials. The plasma frequency varies with the dielectric constant ε_2 of the surroundings and its change can be of several meV in thin QWRs. Since the Coulomb interaction between charged particles is poorly screened in QWRs embedded in high-κ environment, the charged-impurity scattering rate is an increasing function of the dielectric constant ε_2 and changes strongly for $\varepsilon_2 < \varepsilon_1$ in QWRs of small radii and slowly in otherwise. The electron mobility, therefore, is higher in QWRs with low-κ dielectric surroundings ($\varepsilon_2 < \varepsilon_1$), in contrast to the conclusion in previous studies [35,36]. Regarding the confining potential, we have found that the assumption of an infinite height of the potential barrier results in the different radius dependence of the electron screening and the plasma frequency compared to that in QWRs with a finite potential barrier. This difference is mitigated for large QWRs. In addition, the infinite barrier model overestimates the Coulomb scattering rate and, therefore, underestimates the impurity electron mobility for QWRs with small radii. For QWRs with large radii, both models of confining potentials give approximately the same results. This means that the model of infinite potential barrier is applicable to QWRs with large lateral dimension. We hope that our results can be useful for the selection of appropriate dielectric surrounding materials to improve transport properties of semiconductor quantum wires.

Author contributions

The authors contributed equally to the paper and have read and approved the final manuscript.

Data Availability Statement This manuscript has no associated data or the data will not be deposited. [Authors' comment: This is a theoretical study and no experimental data.]

Declarations

Conflict of interest The authors declared that there are no conflicts of interest associated with this publication.

References

1. E. Kapon, D.M. Hwang, R. Bhat, Phys. Rev. Lett. **63**, 430 (1989)
2. X. Duan, Y. Huang, R. Agarwal, C.M. Lieber, Nature **421**, 241 (2003)
3. J.X. Ding, J.A. Zapien, W.W. Chen, Y. Lifshitz, S.T. Lee, X.M. Meng, Appl. Phys. Lett. **85**, 2361 (2004)
4. S. Arai, T. Maruyama, IEEE, J. Sel. Top. Quantum Electron. **15**, 731 (2009)
5. C.Z. Ning, Phys. Status Solidi B **247**, 774 (2010)
6. K.F. Karlsson, H. Weman, M.A. Dupertuis, K. Leifer, A. Rudra, E. Kapon, Phys. Rev. B **70**, 045302 (2004)
7. R. Könenkamp, R.C. Word, C. Schlegel, Appl. Phys. Lett. **85**, 6004 (2004)
8. G. Jacopin, A. de Luna Bugallo, P. Lavenus, L. Rigutti, F..H. Julien, L..F. Zagonel, M. Kociak, C. Durand, D. Salomon, X..J. Chen, J. Eymery, M. Tchernycheva, Appl. Phys. Express **5**, 0141101 (2012)
9. J.W. Kang, B.H. Kim, H. Song, Y.R. Jo, S.H. Hong, G.Y. Jung, B.J. Kim, S.J. Park, C.H. Cho, Nanoscale **10**, 14812 (2018)

10. M.J. Gilbert, R. Akis, D.K. Ferry, Appl. Phys. Lett. **81**, 4284 (2002)
11. S.F. Fischer, G. Apetrii, U. Kunze, D. Schuh, G. Abstreiter, Nat. Phys. **2**, 91 (2006)
12. J. Sone, Semicond. Sci. Technol. **7**, B210 (1992)
13. S. Kasai, H. Hasegawa, Jpn. J. Appl. Phys. **40**, 2029 (2001)
14. Y. Huang, X. Duan, Y. Cui, C.M. Lieber, Nano Lett. **2**, 101 (2002)
15. V. Schmidt, H. Riel, S. Senz, S. Karg, W. Riess, U. Gösele, Small **2**, 85 (2006)
16. K. Trivedi, H. Yuk, H.C. Floresca, M.J. Kim, W. Hu, Nano Lett. **11**, 1412 (2011)
17. X. Duan, Y. Huang, C.M. Lieber, Nano Lett. **2**, 487 (2002)
18. R. Böckle, M. Sistani, P. Staudinger, M.S. Seifner, S. Barth, A. Lugstein, Nanotechnology **31**, 445204 (2020)
19. Y. Cui, Q. Wei, H. Park, C.M. Lieber, Science **293**, 1289 (2001)
20. F. Patolsky, C.M. Lieber, Mater. Today **8**, 20 (2005)
21. M. Tonezzera, N.V. Hieu, Sens. Actuators B **163**, 146 (2012)
22. C.J. Först, C.R. Ashman, K. Schwarz, P.E. Blöchl, Nature **427**, 53 (2004)
23. Z.Y. Deng, S.W. Gu, J. Phys, J. Phys. Condens. Matter **5**, 2261 (1993)
24. M.M. Aghasyan, A.A. Kirakosyan, Phys. E **8**, 281 (2000)
25. H.D. Karki, S. Elagoz, R. Amca, P. Baser, K. Atasever, Phys. E **42**, 1351 (2010)
26. L. Bányai, I. Galbraith, C. Ell, H. Haug, Phys. Rev. B **36**, 6099 (1987)
27. G. Goldoni, F. Rossi, E. Molinari, Phys. Rev. Lett. **80**, 4995 (1998)
28. G. Goldoni, F. Rossi, A. Orlandi, M. Rontani, F. Manghi, E. Molinari, Phys. E **6**, 482 (2000)
29. E.A. Muljarov, E.A. Zhukov, V.S. Dneprovskii, Y. Masumoto, Phys. Rev. B **62**, 7420 (2000)
30. A.F. Slachmuylders, B. Partoens, W. Magnus, F.M. Peeters, Phys. Rev. B **74**, 235321 (2006)
31. A.F. Slachmuylders, B. Partoens, W. Magnus, F.M. Peeters, Phys. Status Solidi C **5**, 2416 (2008)
32. M. Royo, J.I. Climente, J.L. Movilla, J. Planelles, J. Phys, Condens. Matter **23**, 015301 (2011)
33. G. Parascandolo, G. Cantele, D. Ninno, G. Iadonisi, Phys. Rev. B **68**, 245318 (2003)
34. D. Jena, A. Konar, Phys. Rev. Lett. **98**, 136805 (2007)
35. A. Konar, A. Jena, J. Appl. Phys. **102**, 123705 (2007)
36. A. Konar, T. Fang, D. Jena, Phys. Rev. B **84**, 085422 (2011)
37. P.C.M. Machado, F.A.P. Osório, A.N. Borges, Mod. Phys. Lett. B **11**, 441 (1997)
38. A.A. Sousa, T.A.S. Pereira, A. Chaves, J.A. de Sousa, G.A. Farias, Appl. Phys. Lett. **100**, 211601 (2012)
39. M. Abramowitz, I.A. Stegun, *Handbook of Mathematical Functions with Formulas, Graphs, and Mathematical Tables* (National Bureau of Standards, Washington, 1972)
40. H. Ehrenreich, M.H. Cohen, Phys. Rev. **115**, 786 (1959)
41. Q.P. Li, S. Das Sarma, R. Joynt, Phys. Rev. B **45**, 13713 (1992)
42. J.D. Jackson, *Classical Electrodynamics* (Wiley, New York, 1999)
43. T. Vazifehshenas, Phys. Status Solidi A **205**, 1302 (2008)
44. A.R. Goñi, A. Pinczuk, J.S. Weiner, J.M. Calleja, B.S. Dennis, L.N. Pfeiffer, K.W. West, Phys. Rev. Lett. **67**, 3298 (1991)
45. W. Götze, F. Wölfle, Phys. Rev. B **6**, 1226 (1972)